Materials Research Bulletin 60 (2014) 794–801

Contents lists available at ScienceDirect

Materials Research Bulletin

journal homepage: www.elsevier.com/locate/matresbu

Characterization and photocatalytic activity of ZnSe nanoparticles synthesized by a facile solvothermal method, and the effects of different solvents on these properties

Bo Feng [a,*], Jian Cao [a], Jinghai Yang [a,b,**], Shuo Yang [b], Donglai Han [b]

[a] Key Laboratory of Functional Materials Physics and Chemistry of the Ministry of Education, Jilin Normal University, Haifeng Street No. 1301, Siping 136000, PR China

[b] Key Laboratory of Excited State Physics, Changchun Institute of Optics, Fine Mechanics and Physics, Chinese Academy of Sciences, 3888 Eastern Nan-Hu Road, Changchun 130033, PR China

ARTICLE INFO

Article history:
Received 14 June 2014
Received in revised form 6 September 2014
Accepted 24 September 2014
Available online 28 September 2014

Keywords:
A. Nanostructures
A. Semiconductors
B. Chemical synthesis
B. Optical properties
D. Catalytic properties

ABSTRACT

ZnSe nanoparticles were synthesized using a facile solvothermal reaction of zinc nitrate hexahydrate with Se powder, and two types of solvent: (i) ethylene glycol (EG), and (ii) triethanolamine (TEA). The ZnSe nanoparticles obtained using EG solvent, referred to as ZnSe nanoparticles (EG), were measured around 20 nm, while their TEA counterparts, referred to as ZnSe nanoparticles (TEA), were slightly smaller at around 18 nm. The effects of the two solvents on the growth mechanism of the nanoparticles were observed and analyzed. The ZnSe nanoparticles (EG) displayed a weak defect-related emission spectrum between 520 and 580 nm. In contrast, the ZnSe nanoparticles (TEA) displayed a much wider stronger deep defect-related emission spectrum extending from 470 to 630 nm. The photocatalytic activity results demonstrated that ZnSe nanoparticles (TEA) exhibited stronger photocatalytic activity than their EG counterparts by measuring the degradation of Rhodamine B dye under UV light conditions.

1. Introduction

During the past two decades, II–VI semiconductor nanocrystals have been widely studied for their fundamental properties and technological applications, mostly as tunable emitters for biomedical labeling, light emitting diodes, lasers, solar cells and sensors [1–4]. As one of the important Zn-based II–VI semiconductors, zinc selenide (ZnSe) has been considered a suitable material for optoelectronic devices due to its wide direct band gap (2.67 eV) and large exciton binding energy (21 meV) [5,6]. Moreover, due to low absorptivity at infrared wavelengths and high photosensitivity, ZnSe has attracted considerable attention for use in windows, lenses, output couplers, beam expanders, biomedical labels, and optically controlled switching [7,8]. ZnSe nanoparticles can be prepared in a number of ways [9–12]. For example, Zhu et al. reported that ZnSe nanocrystals with a cubic zinc blende crystal structure could be synthesized using a water-in-oil reverse microemulsion method. In our present investigation, a primary goal is to synthesize ZnSe nanoparticles directly from Zn and Se elements, but in such a way that produces a homogeneous nanocrystal size within as short a timeframe as possible, cost-effectively. Among various alternatives, the solvothermal method offers a simple, inexpensive and hence facile low-cost solution [13]. However, it becomes apparent during our literature survey that: (i) very few comparative studies of ZnSe nanoparticles synthesized using different solvents have been reported, (ii) studies have focused mainly on the optical, photoconductive and other physical properties of ZnSe nanostructures, and (iii) little effort has been made to investigate other physical and chemical properties such as photocatalytic activity of ZnSe nanoparticles [14,15].

Semiconductor photocatalysts have attracted considerable attention for quite a while in the fields of catalysis and photochemistry, largely due to their catalytic activity and broad applications in helping to solve important environmental issues such as air and water pollution [16]. Conventional semiconductor photocatalysts like titanium dioxide (TiO_2) exist mostly in the form of oxides. TiO_2 can only absorb UV light and therefore, makes use of only 3–5% of the total solar irradiance that reaches the Earth at UV frequencies [17]. Therefore, exploration of new broader spectrum

* Corresponding author. Tel.: +86 434 3294566; fax: +86 434 3294566.
** Corresponding author.
E-mail addresses: fengbosiping@126.com (B. Feng), jhyang1@jlnu.edu.cn (J. Yang).

http://dx.doi.org/10.1016/j.materresbull.2014.09.071
0025-5408/

photocatalysts with high photocatalytic activity has become a popular focus for current research. Recently, the photocatalytic activity of ZnSe nanostructures has received increased attention from researchers. Qian and co-workers observed the photocatalytic activity of ZnSe nanobelts in the photodegradation of fuchsine acid to be higher than that of TiO_2 nanoparticles under UV light irradiation [18]. This finding is most promising as it enhances the prospects for using ZnSe as an effective catalyst for photocatalytic degradation of organic pollutants.

In this article, we report on a very simple solvothermal method for the controlled synthesis of ZnSe nanoparticles using ethylene glycol (EG) or triethanolamine (TEA) as two alternative solvents. The growth mechanisms of ZnSe nanoparticles obtained by using these two solvents are discussed, along with applicable room temperature photoluminescence spectra and photocatalytic activity measurements. We find that the choice of solvent plays a key role in the growth mechanism of ZnSe nanoparticles. In particular, we observe that when using EG to synthesize ZnSe nanoparticles, synthesis occurs under Zn-rich conditions, while with TEA as the solvent, synthesis occurs under Se-rich conditions. From photocatalytic activity measurements, we observe important differences in the photocatalytic characteristics of the ZnSe nanoparticles synthesized by using the two different solvents. For these tests, the measurements are made using RhB as the degradation dye under UV irradiation. The results are discussed and an explanation for the difference is given.

2. Experimental

2.1. Preparation of ZnSe samples

All chemicals were of analytical grade and used as received, without further purification.

The synthesis of the ZnSe precursors was carried out using the following procedures: $Zn(NO_3)_2{\cdot}6H_2O$ (0.5 mmol) was dissolved in 20 ml of NaOH solution, and then stirring for 40 min. EG or TEA was added into the above solution. After stirring for 1 h, selenium powder (99.95%) (0.5 mmol) was added into the mixed solution. Then after stirring for a further hour, the mixed solution was transferred into the 80-ml Teflon-lined autoclave. The autoclaves were sealed and heated at 180 °C for 24 h. When the reaction was complete the autoclaves were cooled to the room temperature. The products were washed with ethanol and deionized water several times and then separated by centrifugation. They were then dried at 60 °C for 1 h to obtain the precursors. Finally, the precursors were annealed at 350 °C for 2 h to produce the samples.

2.2. Characterizations

The X-ray diffraction (XRD) pattern was collected on a MAC Science MXP-18 X-ray diffractometer using a Cu target radiation source. Energy dispersive X-ray analysis (EDAX) system attached to the scanning electron microscope (SEM) was employed to analyze chemical composition. A transmission electron micrograph (TEM) was taken with a JEM-2100 electron microscope. The specimen was prepared by depositing a drop of the dilute sample solution in 2-propanol on a carbon-coated copper grid and drying at room temperature. UV–vis absorption spectrum was measured on UV-3101PC UV spectrometer. The specimen for the measurement was dispersed in ethanol and placed in a 1 cm quartz cell, and ethanol served as the reference. PL measurement was carried out at room temperature, using 325 nm as the excitation wavelength, and a He–Cd laser as the excitation source. The Raman scattering studies were performed with a 1000B Renishaw micro-Raman system in the back-scattering configuration, and the excitation source was the 514.5 nm line of an Ar^+ laser for which ZnSe was transparent. The beam was focused through a microscope objective on the samples as a 1 μm circular spot.

The photocatalytic activity measurements are as follows: a reaction system that used the as-synthesized products as catalysts and including the RhB aqueous solutions was magnetically stirred in the dark until reaching the adsorption equilibrium of the RhB for the catalyst before exposure to UV irradiation from a 250 W high-pressure Hg lamp (centered at 365 nm). After exposure to the radiation for different intervals, the UV–vis spectrophotometer was used to determine the solution concentration of RhB at room temperature (UV-5800PC, Shanghai Metash Instruments Co., Ltd).

3. Results and discussion

Fig. 1 shows the XRD patterns of the samples obtained by using EG and TEA. The peaks are assigned to the diffractions from (1 1 1), (2 2 0), (3 1 1), (4 0 0), and (3 3 1) planes of the cubic zinc blende phase of ZnSe, respectively, which are in complete agreement with the PDF card (F $\bar{4}$ 3 m, JCPDS file #37-1463). The intensities of the peaks in Fig. 1(a) is slightly stronger than that of the peaks in Fig. 1(b), which indicates that the samples obtained by using EG have better crystallinity. Moreover, no diffraction peaks from Zn or other impurities are observed within the detection limit. The lattice constant 'a' for the cubic structure can be determined from the relations: $1/d^2_{hkl} = (h^2 + k^2 + l^2)/a^2$. The average lattice constant of 'a' for ZnSe sample obtained by using EG is found to be 5.673 Å, while 'a' for ZnSe sample obtained by using TEA is found to be 5.678 Å. Both are slightly larger than the standard value of 5.668 Å. The results indicate that both samples are under tensile strain. The EDAX analysis of the ZnSe samples obtained by using EG and TEA are shown in Fig. 1(c) and (d), respectively, indicating that both samples are composed of the elements Zn and Se (other peaks arise from the Au).

Fig. 2(a) and (b) show the TEM images of the ZnSe nanoparticle samples obtained by using the two solvents chosen for our experiments. In both instances, the ZnSe nanoparticles are observed to have a spherical shape and exhibit a narrow size distribution. The average particle size is approximately 20 nm for EG, as shown in Fig. 2(a), and approximately 18 nm for TEA, as shown in Fig. 2(b). Fig. 2(c) shows the high-resolution TEM (HRTEM) micrographs of ZnSe nanoparticles (EG), evidencing the highly crystalline nature of these ZnSe nanoparticles. The HRTEM images show well-defined lattice planes reflecting a high degree of crystallinity within each single nanocrystal. The observed interplanar distance of 0.33 nm is in excellent agreement with the ZnSe zinc blende structure with a distance of 0.327 nm for the (1 1 1) planes (JCPDS-37-1463). The regular behavior of the lattice fringes inside the nanocrystal further confirms the excellent crystalline nature of these ZnSe nanoparticles (EG). No obvious bulk defects such as stacking faults, dislocations and twining defects are observed. However, in Fig. 2(e), the ZnSe nanoparticles obtained by using TEA are seen to exhibit a high density of structural defects in the form of stacking faults. From these results and theoretical calculations, we conclude that the existence of Se vacancies in the ZnSe nanoparticles is improbable due to the high formation energy, and Zn vacancies and/or Zn interstitials are the most probable causes of point defects in ZnSe nanoparticles [19]. Fig. 2(d) and (f) display the corresponding selected area electron diffraction (SAED) pattern for ZnSe nanoparticles obtained by using EG and TEA, respectively. These figures show a set of sharp spots that clearly reveal the single crystalline nature and cubic phase of the ZnSe nanoparticles, as confirmed by the behaviour of the lattice fringes.

According to the previous research, it was found that the EG worked as both a solvent and a reducing agent in the reaction

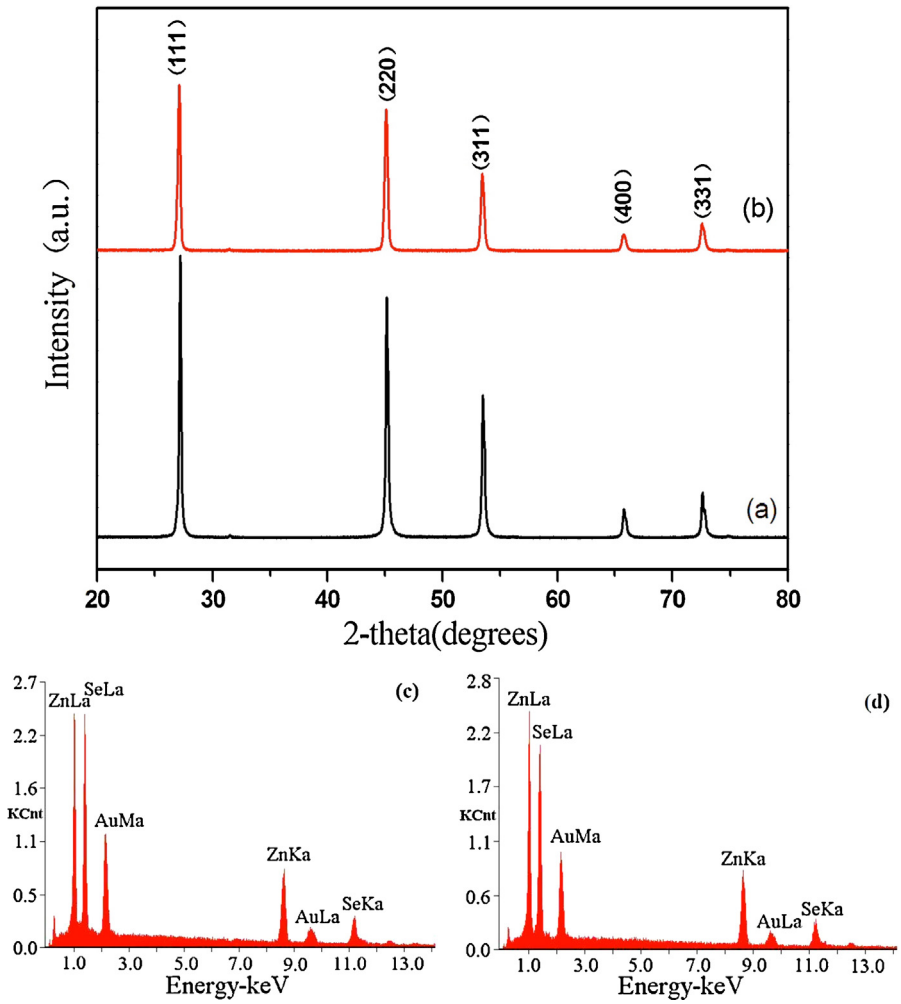

Fig. 1. XRD patterns of ZnSe nanoparticles synthesized using EG (a) and TEA (b), EDAX spectra of ZnSe nanoparticles synthesized using EG (c) and TEA (d).

process of ZnSe nanomaterials synthesis [20,21]. The Se reacts with OH^- ions to form Se^{2-} and SeO_3^{2-} ions [22], and then the SeO_3^{2-} ions are reduced by EG to form Se, while the Se^{2-} ions react with ZnO_2^{2-} to form ZnSe [23]. The chemical reactions to form ZnSe are formulated as follows:

$$Zn(NO_3)_2 = Zn^{2+} + 2NO_3^- \quad (1)$$

$$Zn^{2+} + 4OH^- = Zn(OH)_4^{2-} \quad (2)$$

$$Zn(OH)_4^{2-} = ZnO_2^{2-} + 2H_2O \quad (3)$$

$$3Se + 6OH^- = 2Se^{2-} + SeO_3^{2-} + 3H_2O \quad (4)$$

$$2HOCH_2CH_2OH = 2CH_3CHO + 2H_2O \quad (5)$$

$$2CH_3CHO + SeO_3^{2-} = 2CH_3COO^- + Se + H_2O \quad (6)$$

$$Se^{2-} + ZnO_2^{2-} + 2H_2O = ZnSe + 4OH^- \quad (7)$$

In the reaction system, the four reaction step is slow and determines the formation velocity or rate of synthesis of the ZnSe nanoparticles. This formation process is illustrated in Fig. 3(a). After the initial nucleation, the ZnSe monomers grow into ZnSe nanoparticlels as this represents a minimum energy state. The formation and growth of ZnSe nanoparticles obtained by using EG is slow for the above mentioned reason.

In ZnSe nanoparticle synthesis using TEA, the TEA serves as both an alkaline and complexing agent [24,25]. Because the N atom of TEA has an electron pair that can combine with a proton, an aqueous solution of TEA is weakly alkaline. During the reaction process, Zn^{2+} firstly reacts with OH^- to form $Zn(OH)_2$, TEA then works as an organic complexing agent between TEA and $[Zn(OH)_2]_n$ to form coordination complexes $[Zn(OH)_2TEA]_n$. A schematic of this process is shown in Fig. 3(b). The possible growth mechanism can be described as the following:

$$Zn(NO_3)_2 = Zn^{2+} + 2NO_3^- \quad (1)$$

$$Zn^{2+} + 2OH^- = Zn(OH)_2 \quad (2)$$

$$[Zn(OH)_2]_n + nTEA = [Zn(OH)_2TEA]_n \quad (3)$$

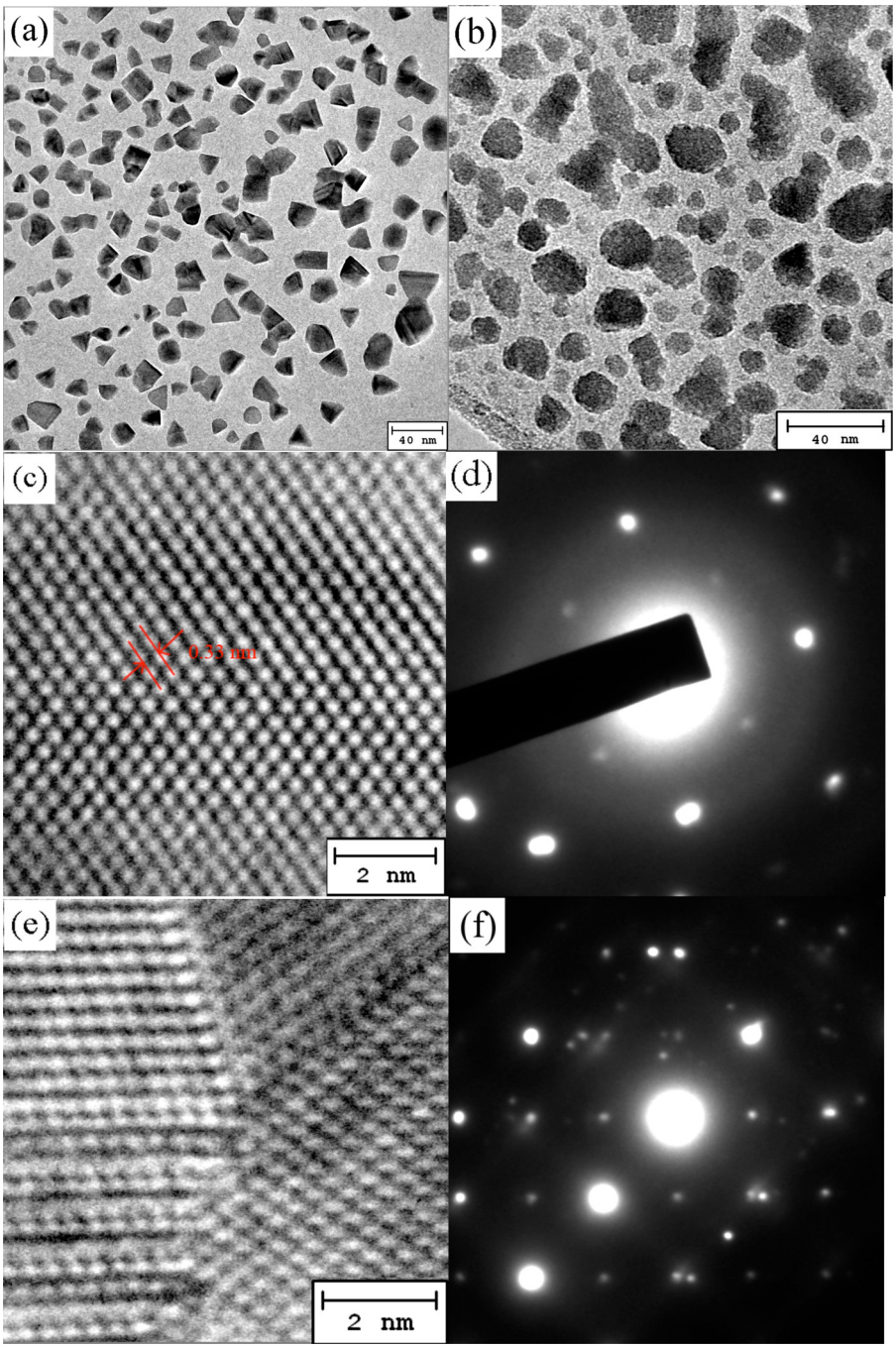

Fig. 2. TEM image (a), High-resolution TEM image (c), SAED patterns (d) of ZnSe nanoparticles (EG) TEM image (b), High-resolution TEM image (e), SAED patterns (f) of ZnSe nanoparticles (TEA).

$$Zn(OH)_2 + 2OH^- + TEA = [Zn(OH)_4{}^{2-}TEA] \quad (4)$$

$$[Zn(OH)_4{}^{2-}TEA] + Se = ZnSe + 4OH^- + TEA \quad (5)$$

Fig. 4 shows the UV–vis spectra of the ZnSe nanoparticles. The characteristic absorption peaks of the samples appeared in the range 420–460 nm. The peak position reflects the band gap of the ZnSe nanoparticles. The absorption maxima for the ZnSe nanoparticles is 428 nm (EG), 420 nm (TEA) respectively, which display blue-shift as compared to the bulk ZnSe (465 nm) indicating the formation of nanomaterials. The small blue-shift in the absorption peak position may be related to the size of the nanoprticles. It is well known that ZnSe is a direct gap semiconductor. The optical band gap 'E_g' can be calculated using the following relation:

$$\alpha = \frac{A(h\nu - E_g)^n}{h\nu}$$

where A is a constant and n is a constant, equal to 1/2 for direct band gap semiconductor. We found that the bandgap of the ZnSe nanoparticles is 2.897 eV (EG), and 2.952 eV (TEA) respectively.

The room temperature PL spectrum of the as-synthesized ZnSe nanoparticles obtained by using EG and TEA is shown in Fig. 5.

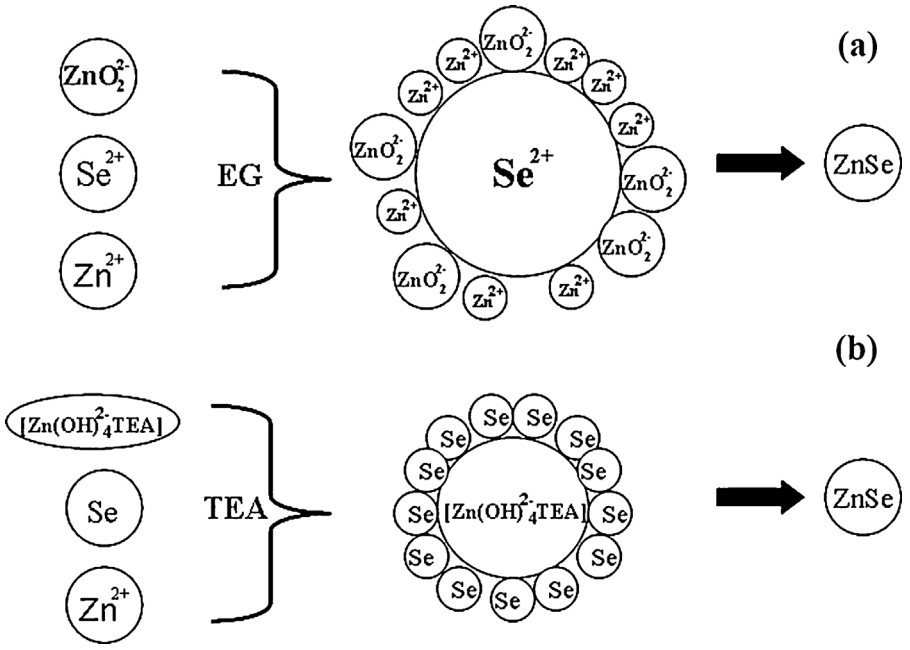

Fig. 3. Schematic illustration of the growth process of ZnSe nanoparticles synthesized using EG (a) and TEA (b).

Fig. 5(a) shows the PL spectrum for ZnSe nanoparticles (EG). The spectrum exhibits a strong and stable blue emission band centered at 445 nm and a very weak emission band from 520 to 580 nm is also observed. The strong blue emission band centered at 445 nm is usually attributed to the near-band edge (NBE) emission for ZnSe [26], while the weaker emission band from 520 to 580 nm represents deep defect-related emission [27]. In contrast, the PL spectrum for ZnSe nanoparticles (TEA) shown in Fig. 5(b) exhibits a weak blue NBE emission band centered at 448 nm [28], and a very strong broad deep defect-related emission band extending from 470 to 650 nm [29]. The NBE emission peak of the ZnSe nanoparticles can be estimated to be shifted toward higher energy, when compared to the 2.67 eV (corresponding to 465 nm) band gap of the bulk ZnSe material. This observation is in accordance with the previous research finding that ZnSe nanocrystals exhibit size-dependent photoluminescence properties [30,31].

It is known that the lattice strain increases with decreasing the particle size. Consequently, it is also found that the band gap energy of semiconductor nanocrystals increases with the decrease in particle size due to the imperfect coordination and strain in the self-equilibrium state [32]. The lattice strain would also have an effect on the observed blue shift in the NBE emission peak in our experiments. We believe that the blue shifts in the photoluminescence emission spectra are caused by the size-dependent lattice strain, which is perhaps a major contributor to the observed variation in band gap energy.

During the growth process of the ZnSe nanoparticles (EG), an excess in the concentration of Zn^{2+} ions occurs during the reaction process due to the slowness of the reaction. Therefore, the ZnSe nanoparticles (EG) are obtained under Zn-rich conditions and are of high optical quality. In contrast, during ZnSe nanoparticles (TEA)

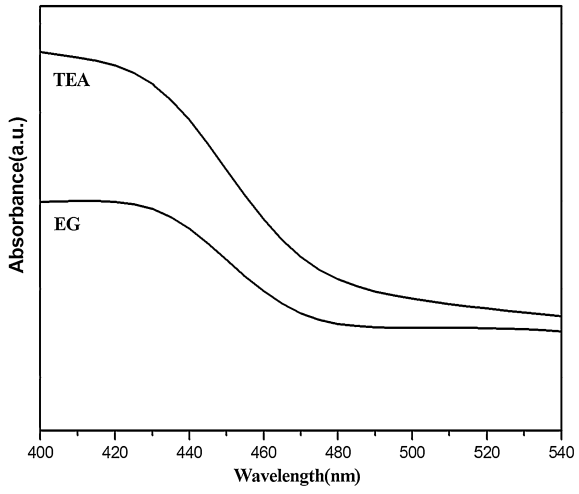

Fig. 4. UV–vis absorption spectra of the ZnSe nanoparticles.

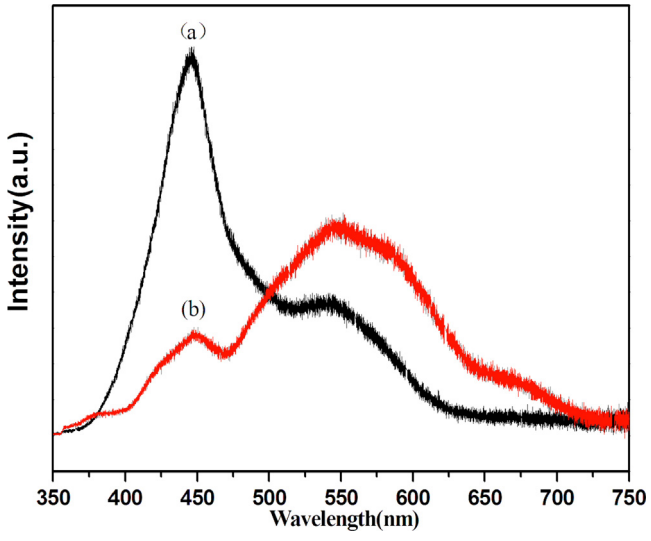

Fig. 5. Room-temperature PL spectrum (excited at 325 nm) of ZnSe nanoparticles synthesized using EG (a) and TEA (b).

synthesis, the Zn^{2+} ions are in the form of $[Zn(OH)_4{}^{2-}TEA]$, so the ZnSe nanoparticles (TEA) are obtained under Se-rich conditions. Consequently, the low concentration of Zn vacancies probably accounts for the lower intensity of the deep defect emission peak for the EG case. It should be noted that the ZnSe nanoparticles (TEA) obtained under Se-rich conditions contain a high density of structural defects. So, synthesis under Se-rich conditions most likely introduces a high concentration of defects, which in turn may be responsible for the higher deep defect emission for ZnSe nanoparticles (TEA) [33].

During the synthesis of ZnSe nanoparticles, various point and extended defects can be formed, leading to the observed stacking faults and strong defect-related emissions in the PL spectra [34]. The origin of the deep defect-related emission is attributed to recombination of a donor–acceptor pair involving Zn vacancies and Zn interstitials. In binary compounds like ZnSe, various forms of intrinsic point defects may occur, having appropriate positive or negative charges. The vacancies and interstitials of Zn, having different charge states, can create different localized levels within the band gap, and can therefore combine to form donor–acceptor pairs. Se vacancies and Zn interstitials introduce energy levels closer to the edge of the conduction band and hence act as donor states. In constrast, Zn vacancies and Se interstitials introduce levels closer to the valence band edge and act as acceptor states. Synthesizing the ZnSe nanoparticles by using TEA would cause an increase in the net vacancy concentration, whereas synthesizing them by using EG would have quite the opposite effect. Therefore, the high density of structural defects can be attributed to an increased net defect concentration. According to Philipose [35], ZnSe nanowires grown under Zn-rich conditions had a strong NBE emission, whilst nanowire grown under Se-rich conditions had a strong deep defect emission. This is in accordance with our results and lends support to our analysis and general conclusions.

Generally, the intensity ratio of NBE emission band to defect-related emission band is regarded as an indicator of the crystallinity of semiconductor materials. The materials have much better crystallization according to the larger intensity ratio. The relative PL intensity ratio of NBE emission (I_{NBE}) to defect-related emission (I_{DRE}) of ZnSe nanoparticles obtained by using EG and TEA is estimated to be about 2.642 and 0.123, respectively. It can be seen that the ZnSe nanoparticles by using EG have much better crystallization according to the larger intensity ratio.

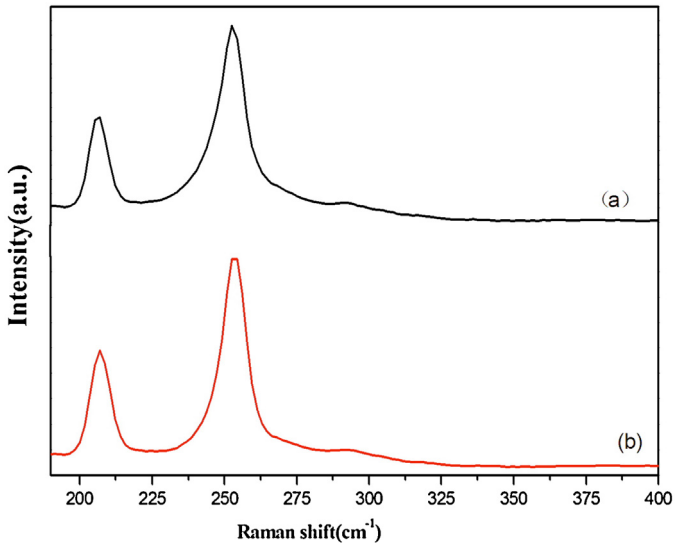

Fig. 6. Raman spectrum of ZnSe nanoparticles synthesized using EG (a) and TEA (b), 514.5 nm excitation.

Raman scattering is very sensitive to the microstructure of nano-sized materials. Fig. 6 shows a typical room-temperature Raman spectrum of the ZnSe nanoparticles obtained by using EG and TEA. As seen from Fig. 6(a) for ZnSe nanoparticles (EG), two Raman peaks centered at 206 and 252 cm^{-1} are observed, which are attributed to the transverse optic (TO) and longitudinal optic (LO) phonon modes of ZnSe, respectively. In Fig. 6(b) for ZnSe nanoparticles (TEA), two Raman peaks centered at 206 and 253 cm^{-1} are observed. The TO and LO phonon modes of ZnSe nanoparticles obtained by using the two solvents showed a clear shifting toward the low frequency relative to bulk values, probably due to their small size and high surface area.

In order to investigate the photocatalytic activity of the ZnSe nanoparticles, RhB is chosen as the photocatalytic degradation dye since it is a good model compound as a target pollutant that is stable under UV irradiation [36]. Prior to the photocatalytic reaction, the RhB solutions are first photolyzed in the absence of the photocatalysts to determine their stability. The results show that the dyes exhibit almost no decomposition even after long illumination with UV light. In addition, the concentrations of RhB exhibit virtually no change under dark conditions after the ZnSe and RhB solutions reach adsorption–desorption equilibrium. Therefore, the presence of photocatalysts and illumination is considered necessary for efficient degradation.

The time-dependent absorption spectra during UV irradiation of RhB solutions containing samples of ZnSe nanoparticles (EG) and (TEA), respectively, are illustrated in Fig. 7(a) and (b). Curves of degradation efficiency versus reaction time for ZnSe nanoparticles are shown in Fig. 7(c). RhB shows a maximum absorption band at 550 nm. It can be seen that the maximum absorbance at 550 nm decreases with the irradiation time, and the maximum absorbance disappears almost completely after irradiation for about 3 h. The loss of absorbance is due to the destruction of the RhB, since no new peak is observed thereby indicating that the RhB has decomposed. The absorption intensity of the peak is reduced by about 84% and 92% in the presence of ZnSe nanoparticles obtained by using EG and TEA, respectively, revealing that the ZnSe nanoparticles are effective photocatalysts due to their high catalytic activity in the degradation of RhB. The catalytic superiority of the ZnSe nanoparticles can be assigned to their large specific surface area and the high catalytic activity of the photo-induced carriers. It is generally accepted that the catalytic process is related mainly to the adsorption and desorption of molecules on the surface of the catalyst [37,38]. The high specific surface area results in more unsaturated surface coordination sites being exposed to the solution.

Additionally, as is well-known, optimum band gap choice plays a key role in the photocatalytic activity of semiconductors. Electron–hole pair generation is dependent on the band gap of ZnSe. The blue-shift of the NBE emission peak appears to offer a useful means for obtaining increased electron–hole pair generation. The results show that the hydroxyl ($OH^{\bullet}$) groups present in nanophotocatalysts assist in higher electron–hole pair generation (as compared with bulk photocatalysts), thereby enabling them to capture the photo-produced h^+ and preventing recombination of the h^+ and e^-, which consequently improves the photocatalytic activity.

Furthermore, the PL analyses of the prepared samples of ZnSe nanoparticles may explain why the ZnSe nanoparticles (TEA) show higher photocatalytic activity than their EG counterparts. Fig. 5 clearly shows that the defect-related emission for ZnSe nanoparticles (TEA) is much stronger than that for ZnSe nanoparticles (EG), suggesting increased defects generation in the nanoparticles is obtained by using TEA. The I_{NBE}/I_{DRE} ratio also indicates more defects in the ZnSe nanoparticles (TEA) samples. The same conclusion can be drawn from the TEM results. It is known that Zn vacancies act as the acceptor species while Zn interstitials as the donor species. The photoelectrons and photoholes (electron–hole pairs) can be

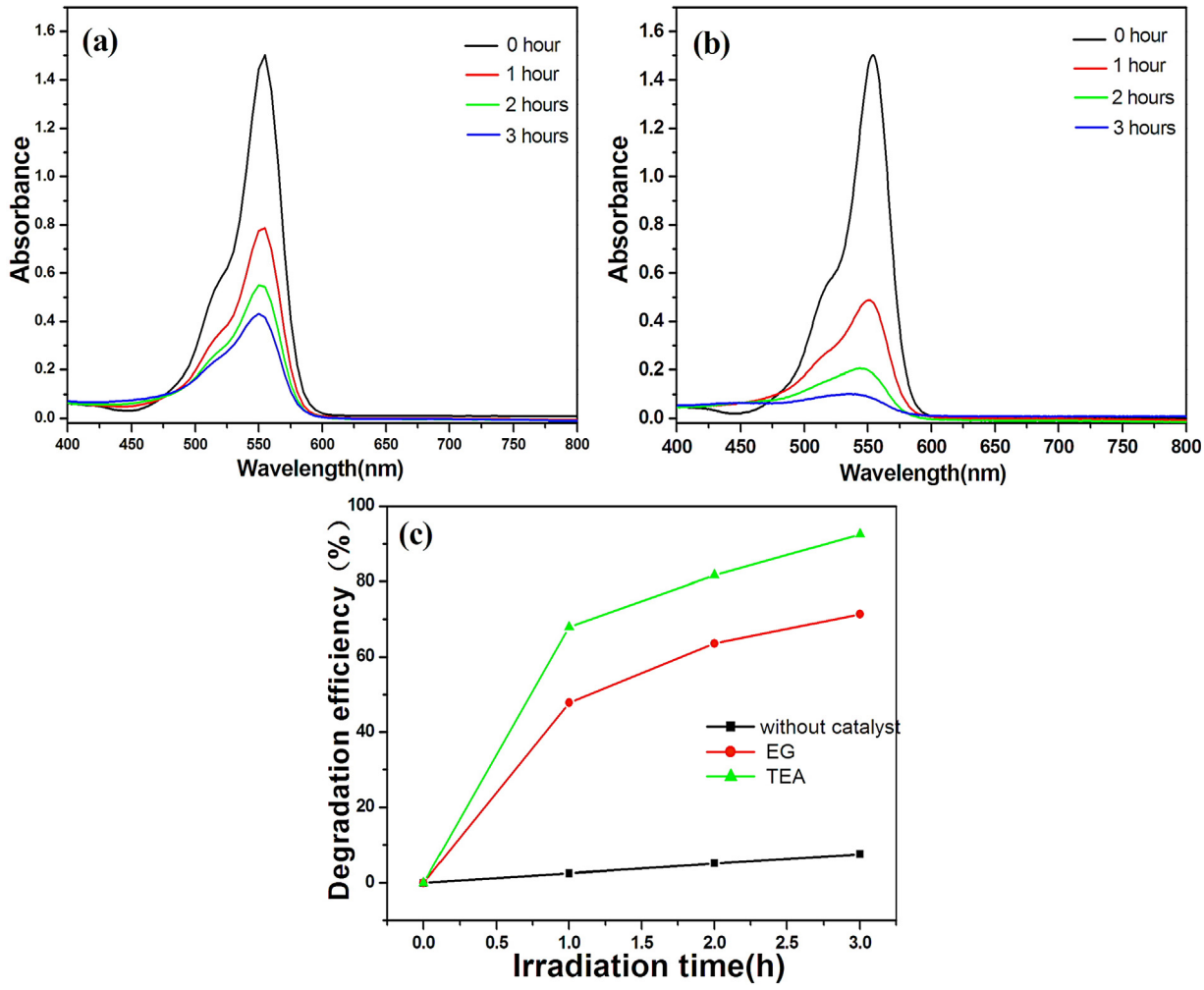

Fig. 7. (Color online) Adsorption changes of RhB aqueous in the presence of ZnSe nanoparticles synthesized using the two solvents under irradiation with UV light at different intervals, (a) EG and (b) TEA, (c) Degradation efficiency versus reaction time for ZnSe nanoparticles synthesized using EG and TEA.

generated when semiconductor material is irradiated at certain frequencies. It is generally accepted that the photocatalytic activity of semiconductor material can be increased by increasing electron–hole pairs generation [39]. Meanwhile, the chance of generation and recombination of electron–hole pairs is equal. When photoelectrons are captured by defects in ZnSe nanoparticles, the recombination of photoelectrons and photoholes can be effectively inhibited. So, defects may serve as recombination centers for photoexcited electron–hole pairs during photocatalysis, implying that the decrease in the occurrence of defects constitute a decrease in photocatalytic activity [40]. We conclude therefore that ZnSe nanoparticles obtained by using TEA with lower I_{NBE}/I_{DRE} ratio should exhibit higher photocatalytic activity, which is what we observe experimentally.

4. Conclusion

In summary, ZnSe nanoparticles with a cubic zinc blende structure have been synthesized through a facile solvothermal method. The ZnSe nanoparticles obtained by using EG are about 20 nm in size, while the ZnSe nanoparticles obtained by using TEA are about 18 nm. Possible reaction and growth mechanisms have been presented, which indicate that the choice of solvent plays an important role not only in the formation of ZnSe nanoparticles but also in the associated physical properties and photocatalytic activity of the synthesized nanoparticles. The room temperature photoluminescence measurements show that the ZnSe nanoparticles (EG) display a strong near-band edge emission peak at 445 nm and a weak deep defect-related emission from 520 to 580 nm. Because the ZnSe nanoparticles (EG) are obtained under Zn-rich conditions, the low concentration of Zn vacancies probably accounts for the lower intensity of the deep defect emission peak. However, the ZnSe nanoparticles (TEA) display a weak near-band edge emission peak at 448 nm and a strong deep defect-related emission from 470 to 630 nm. The ZnSe nanoparticles (TEA) obtained under Se-rich conditions contain a high density of structural defects which could be responsible for the strong deep defect emission. In the Raman spectrum, relative to the bulk crystals of ZnSe, the LO and TO phonon peaks of the ZnSe nanoparticles both shift toward lower frequencies, probably due to their small size and high surface area. Based on our measurements of the degradation of RhB under UV light irradiation using both samples of ZnSe nanoparticles, the nanoparticles synthesized using TEA exhibit higher photocatalytic activity than their EG counterparts.

Acknowledgments

This work was financially supported by the National Natural Science Foundation of China (Grant No. 61178074,61008051, 61378085), Program for the development of Science and Technology of Jilin province (Item No. 201205078, 201215225).

References

[1] L. Carbone, P. Davide Cozzoli, Nano Today 5 (2010) 449–493.
[2] B. Goswami, S. Pal, C. Ghosh, P. Sarkar, J. Phys. Chem. C 113 (2009) 6439–6443.
[3] G. Colibaba, M. Caraman, I. Evtodiev, S. Evtodiev, E. Goncearenco, D. Nedeoglo, N. Nedeoglo, J. Lumin. 145 (2014) 237–243.
[4] J. Li, X. Li, R. Yang, L. Qu, P. de, B. Harrington, Anal. Chim. Acta 804 (2013) 76–83.
[5] L. Zhang, H. Yang, J. Yu, F. Shao, L. Li, F. Zhang, H. Zhao, J Phys. Chem. C 113 (2009) 5434–5443.
[6] A.P.P. Gonzalez, H.G.C. Lora, L.D.L. Carreño, H.M. Martínez, N.J.T. Salcedo, J. Phys. Chem. Solids 75 (2014) 713–725.
[7] J. Archana, M. Navaneethan, Y. Hayakawa, S. Ponnusamy, C. Muthamizhchelvan, Mater. Res. Bull. 47 (2012) 1892–1897.
[8] A.L. Weaver, D.R. Gamelin, J. Am. Chem. Soc. 134 (2012) 6819–6825.
[9] X. Wang, J. Zhu, Y. Zhang, J. Jiang, S. Wei, Appl. Phys. A 99 (2010) 651–656.
[10] J. Zhu, Y. Koltypin, A. Gedanken, Chem. Mater. 12 (2000) 73–78.
[11] M. Shakir, S.K. Kushwaha, K.K. Maurya, G. Bhagavannarayana, Solid State Commun. 149 (2009) 2047–2049.
[12] L. Yang, R. Xie, L. Liu, D. Xiao, J. Zhu, J. Phys. Chem. C 115 (2011) 19507–19512.
[13] S. Jana, I.C. Baek, M.A. Lim, S. Seok II, J. Colloid Interface Sci. 322 (2008) 473–477.
[14] Y. Badr, M.A. Mahmoud, Spectrochim. Acta Part A 65 (2006) 584–590.
[15] D. Sarigannis, J.D. Peck, G. Kioseogiou, A. Petrou, T.J. Mountaiaris, Appl. Phys. Lett. 80 (2002) 4024–4026.
[16] M.R. Hoffmann, S.T. Martin, W. Choi, D.W. Bahnemann, Chem. Rev. 95 (1995) 69–96.
[17] R. Wang, G. Jiang, Y. Ding, Y. Wang, X. Sun, X. Wang, W. Chen, Appl. Mater. Interfaces 3 (2011) 4154–4158.
[18] S. Xiong, B. Xi, C. Wang, G. Xi, X. Liu, Y. Qian, Chem. Eur. J. 13 (2007) 7926–7932.
[19] K. Shahzad, J. Petruzzello, D.J. Olego, D.A. Cammack, J.M. Gaines, Appl. Phys. Lett. 57 (1990) 2452–2454.
[20] Y.G. Sun, Y.D. Yin, B.T. Mayers, T. Herricks, Y.N. Xia, Chem. Mater. 14 (2002) 4736–4745.
[21] J.W. Wang, X. Wang, Q. Peng, Y.D. Li, Inorg. Chem. 43 (2004) 7552–7556.
[22] C. Wang, W.X. Zhang, X.F. Qian, X.M. Zhang, Y. Xie, Y.T. Qian, Mater. Chem. Phys. 60 (1999) 99–102.
[23] L. Zhang, H. Yang, X. Xie, F. Zhang, L. Li, J. Alloys Compd. 473 (2009) 65–70.
[24] H.K. Sadekar, A.V. Ghule, R. Sharma, Composites: Part B 44 (2013) 553–557.
[25] T. Ban, T. Sakai, Y. Ohya, Cryst. Res. Technol. 42 (2007) 849–855.
[26] B.Y. Geng, Q.B. Du, X.W. Liu, J.Z. Ma, X.W. Wei, Appl. Phys. Lett. 89 (2006) 033115.
[27] A. Othonos, E. Lioudakis, D. Tsokkou, U. Philipose, Harry E. Ruda, J. Alloys Compd. 483 (2009) 600–603.
[28] C. Ye, X. Fang, Y. Wang, P. Yan, J. Zhao, L. Zhang, Appl. Phys. A 79 (2004) 113–115.
[29] Y. Jiang, X.M. Meng, W.C. Yiu, J. Liu, J.X. Ding, C.S. Lee, S.T. Lee, J. Phys. Chem. B 108 (2004) 2784–2787.
[30] D.J. Kim, K.K. Koo, Cryst. Growth Des. 9 (2009) 1153–1157.
[31] Z.T. Deng, F.L. Lie, S.Y. Shen, I. Ghosh, M. Mansuripur, A. Muscat, J. Langmuir 25 (2009) 434–442.
[32] Z.M. Zhu, A. Zhang, G. Quyang, G.W. Yang, J. Phys. Chem. C 115 (2011) 6462–6466.
[33] U. Philipose, S. Yang, T. Xu, H.E. Ruda, Appl. Phys. Lett. 90 (2007) 063103.
[34] C.A. Smith, H.W.H. Lee, V.J. Leppert, S.H. Risbud, Appl. Phys. Lett. 75 (1999) 1688–1690.
[35] U. Philipose, T. Xu, S. Yang, P. Sun, H.E. Ruda, Y.Q. Wang, K.L. Kavanagh, J. Appl. Phys. 100 (2006) 084316.
[36] J. Muto, J. Phys. Chem. 80 (1976) 1342–1346.
[37] J. Huang, M. Yang, C. Gu, M. Zhai, Y. Sun, J. Liu, Mater. Res. Bull. 46 (2011) 1211–1218.
[38] A.D. browski, Adv. Colloid Interface Sci. 93 (2001) 135–224.
[39] B. Xin, L. Jing, Z. Ren, B. Wang, H. Fu, J. Phys. Chem. B 109 (2005) 2805–2809.
[40] Y. Liu, W.J. Son, J. Lu, B. Huang, Y. Dai, M.H. Whangbo, Chem. Eur. J. 17 (2011) 9342–9349.